

UNIVERSITY OF SOUTHAMPTON

**Disc Winds Matter: Modelling
Accretion and Outflow on All Scales**

by

James Matthews

A thesis submitted in partial fulfillment for the
degree of Doctor of Philosophy

in the
Faculty of Physical Sciences and Engineering
Department of Physics & Astronomy

May 2016

“Here, on the edge of what we know, in contact with the ocean of the unknown, shines the mystery and the beauty of the world.

And it’s breathtaking.”

Seven Brief Lessons on Physics, Carlo Rovelli

“Good enough for government work.”

Christian Knigge

UNIVERSITY OF SOUTHAMPTON

Abstract

Faculty of Physical Sciences and Engineering
Department of Physics & Astronomy

Doctor of Philosophy

by James Matthews

Outflows are ubiquitous in accreting systems across 10 orders of magnitude in mass. They can take the form of highly collimated radio jets, or less collimated, mass loaded winds emanating from the accretion disc. Perhaps the most spectacular evidence for accretion disc winds is the blue-shifted, broad absorption lines (BALs) in UV resonance lines, seen in cataclysmic variables (CVs) and approximately 20% of quasars. In addition to directly producing absorption in the spectrum, it is possible that accretion disc winds may significantly affect the line and continuum *emission* from CVs and quasars – as a result, they may even dominate the spectral appearance of such objects. When one considers that disc winds are also a possible mechanism for AGN feedback, it becomes clear that understanding the physics and true spectral imprint of these winds is of wide-ranging astrophysical significance.

In this thesis I use the confusingly named Monte Carlo radiative transfer (MCRT) code, PYTHON, to conduct a series of MCRT and photoionization simulations designed to test simple biconical disc wind models. I provide a detailed description of these methods, focusing particularly on the macro-atom implementation developed by Leon Lucy. First, I apply them to the optical spectra of CVs. Second, I conduct tests of quasar unification models. Finally, informed by the previous study, I use Sloan Digital Sky Survey and Hubble Space Telescope data to test the models in an empirical way, by using emission line equivalent widths as a probe of unification geometries.

Overall, the work presented here suggests that *disc winds matter*. They not only act as a spectral ‘filter’ for the underlying accretion continuum, but may actually dominate the emergent spectrum from accreting objects. As a result, unveiling their driving mechanisms, mass-loss rates, and ionization structure is an important goal for the astronomical community.

Contents

Abstract	ii
List of Figures	v
List of Tables	vi
1 Quasar Emission Lines as Probes of Orientation and Unification	1
1.1 Introduction	1
1.2 Data Sample	2
1.3 The Angular Distribution of Emission from an Accretion Disc	6
1.3.1 Standard Thin Disc Models	6
1.3.2 Including GR, Comptonisation and Opacity Effects	6
1.4 Predicted EW Distributions Compared to Observations	7
1.4.1 Fitting the Quasar Distribution	7
1.4.2 Comparing non-BAL and BAL Distributions	9
1.4.3 EW[O III] in LoBAL quasars	13
1.4.4 Broad Emission Lines in HiBAL quasars	14
1.5 Discussion	14
1.5.1 Eigenvector 1	17
1.5.2 Radio Observations	18
1.5.3 Polarisation	19
1.5.4 Theoretical Considerations	19
1.6 Conclusions	21
2 Conclusions and Future Work	23
2.1 Suggestions for Future Work	26
2.1.1 CVs as Accretion and Outflow Laboratories	26
2.1.2 Improving the Treatment of Clumping	26
2.1.3 Improving Atomic Models	27
2.1.4 Using Radiative Transfer to Test	27
2.1.5 Obtaining Reliable Orientation Indicators	27
2.1.6 Placing BAL Quasars on the Eigenvector 1 Parameter Space	27
2.2 Closing Remarks	27

Bibliography	28
---------------------	-----------

List of Figures

1.1	BH mass and Eddington fraction for the BAL samples plotted over the overall quasar sample from S11.	3
1.2	Histograms of equivalent widths for three emission lines from the two different samples.	4
1.3	Monochromatic continuum luminosities from AGNSPEC and classical thin disc models.	8
1.4	Theoretical Ew distributions from the numerical experiment described in section 1.4.1 for a few different maximum angles. The results in the top panel use the same intrinsic distribution as Model 1 from R11 (shown in black), whereas the bottom panel shows the distributions obtained from a narrower intrinsic Gaussian. By the time the maximum angle is limited to around 70° the cutoff is clear even at moderate values of EW.	10
1.5	The EW distribution of quasars in the R11 sample (red errorbars) and the best fit model with a maximum viewing angle of 84°.	11
1.6	The geometry of the toy model used to carry out the Monte Carlo simulations	12
1.7	Heatmap showing the results	14
1.8	Contour plots from the Monte Carlo simulations.	15
1.9	Contour plots from the Monte Carlo simulations.	16
1.10	Eigenvector 1 for BAL and non-BAL quasars.	18
1.11	LoBAL fraction compared to mean LoBAL fraction in Eigenvector 1 space.	19
1.12	<i>Top:</i> Polarisation percentages as a function of measured inclination from Marin et al. (2015) for Type I and Type II AGN. <i>Bottom:</i> Histograms of polarisation percentages for BAL quasars from Schmidt et al. (1999) together with the Marin et al. (2015) AGN sample.	20

List of Tables

1.1 Eigenvector 1 correlation coefficients	17
--	----

Dedicated to my family. Thanks for being awesome....

Chapter 1

Quasar Emission Lines as Probes of Orientation and Unification

This chapter is based on a paper in preparation:

Matthews J. H., Knigge C., ‘Quasar Emission Lines as Probes of Orientation and Unification’, to be submitted to MNRAS.

1.1 Introduction

In the previous chapter, I presented tests of geometric unification models using MCRT and photoionization simulations. One of the key results from that analysis is that trends with inclination prohibit models with equatorial outflows matching observations, as the EW of the emission lines tend to increase with inclination. This trend has clear implications for the geometries of BAL outflows; the viewing angle may determine many of the selection effects at work and must therefore be understood before the true covering factor of BAL outflows can be accurately determined. The covering factor and opening angle of the outflow are important quantities to measure in order to calculate the feedback efficiency (e.g. [Borguet et al. 2012](#)), and make inferences about the outflow physics (e.g. [Proga 2005](#)).

Unlike in galactic accretion disc systems, measuring inclinations for quasars and AGN is notoriously difficult, and obtaining reliable orientation indicators is thus an important

observational goal for the community. Perhaps as a result of this problem, directly opposing geometries have been proposed for BAL outflows (see section ??). Here, I use observational data from the Sloan Digital Sky Survey to constrain the inclinations of BAL quasars. Similar attempts have been made previously with different diagnostics; for example, by considering radio properties (Zhou et al. 2006; DiPompeo et al. 2012b), polarisation (Brotherton et al. 2006) and general emission line properties (DiPompeo et al. 2012a).

This chapter is structured as follows. First, I describe the data sample and selection criteria being used. I begin by simply examining the distributions of the EW of the O III 5007Å emission line, EW[O III], and comparing the BAL and non-BAL quasar distributions. In section 1.3 I review the angular distribution of continuum emission one would expect from simple α -disc models, as well as exploring the same quantity in more advanced disc models computed with AGNSPEC. I then use these theoretical angular distributions applied to a simple toy model in section 1.4, and conduct MC simulations in an attempt to fit the observed BAL and non-BAL quasar distributions of EW[O III], using a similar approach to Risaliti et al. (2011, hereafter R11). In section 1.5 I discuss the results in the context of radio and polarisation measurements of AGN, as well as exploring the location of BAL quasars in ‘Eigenvector 1’ parameter space. Finally, in section 1.6, I summarise the findings.

1.2 Data Sample

The data sample is based upon the Shen et al. (2011, hereafter S11) catalog of 105,783 quasars from the The Sloan Digital Sky Survey (SDSS) Data Release 7 (DR7). As I will use emission line diagnostics in this study, this sample must be further divided according to which emission lines are present in the SDSS wavelength range at a given redshift. Sample A contains all quasars within the redshift range $0.35 < z < 0.83$, such that the Mg II 2800A and O III 5007Å line EWs are both measured, and Mg II BAL identification is possible. Sample B contains all quasars within the redshift range $1.45 < z < 2.28$, such that the EWs and presence of BALs in Mg II 2800A and CIV 1550A are both measurable. The details of these samples are shown in table 1.

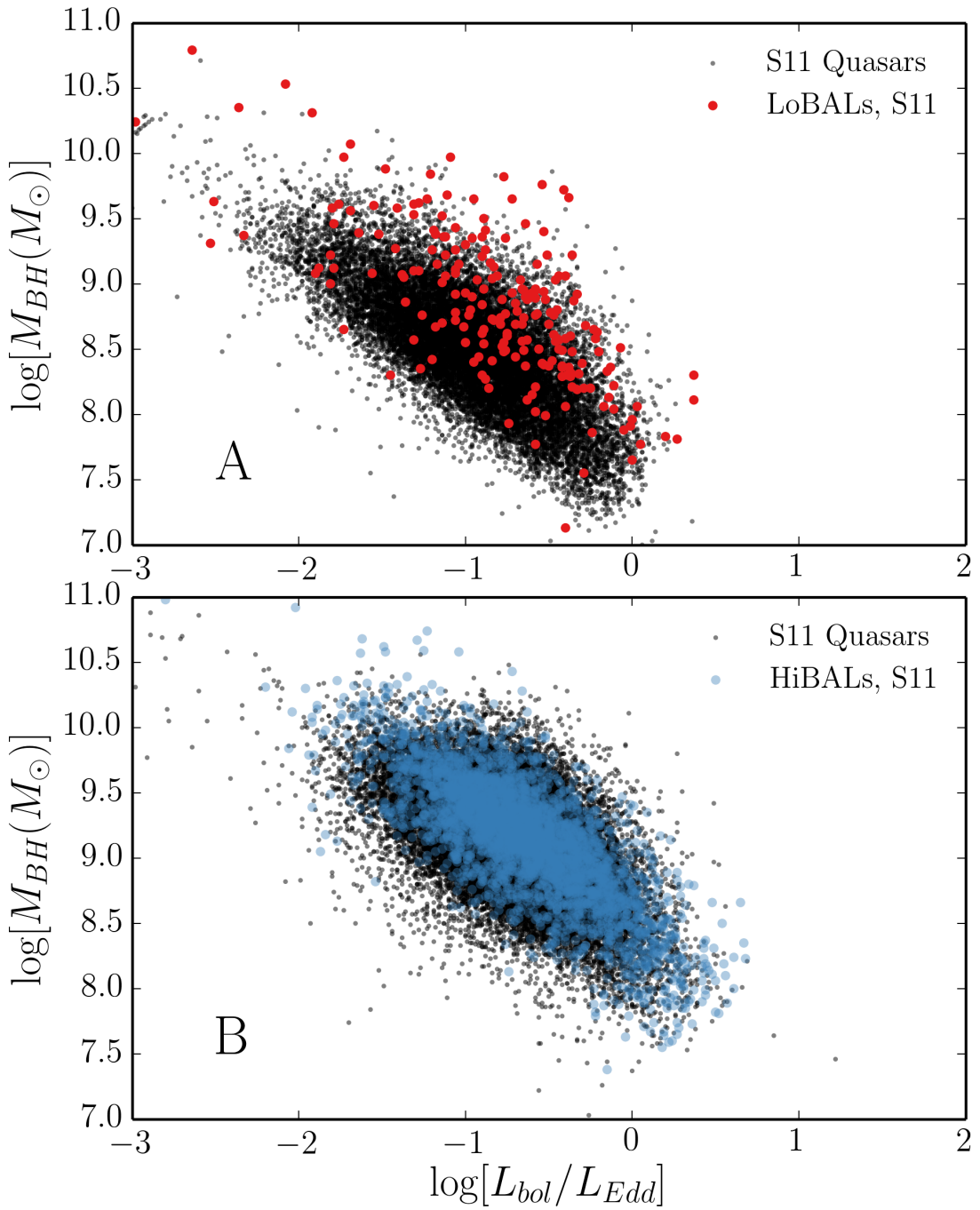


FIGURE 1.1: BH mass and Eddington fraction for the BAL samples plotted over the overall quasar sample from S11.

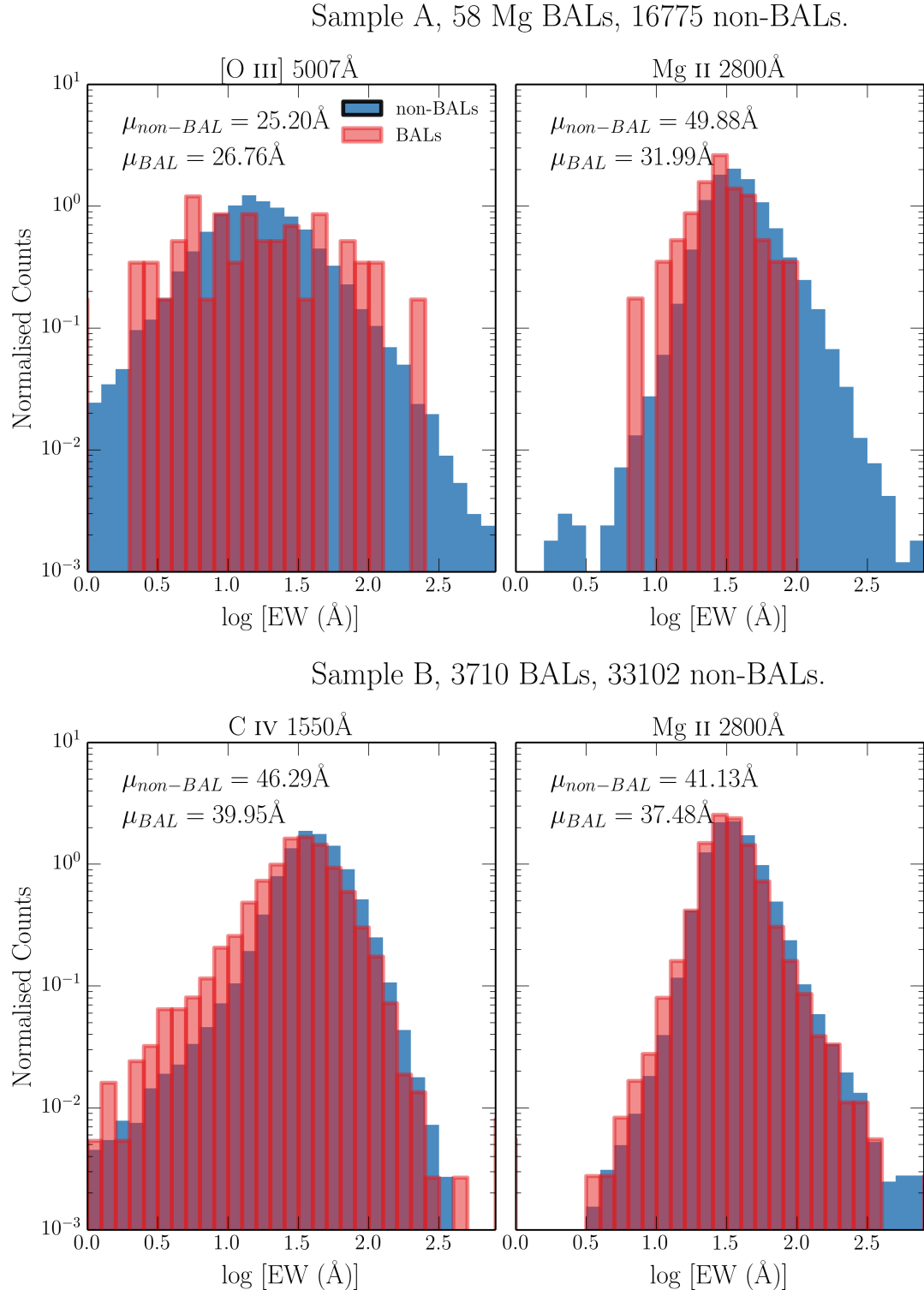


FIGURE 1.2: Histograms of equivalent widths for three emission lines from the two different samples.

In attempting to draw broad conclusions about unification models as a whole, we would like to be able to construct a large homogenous dataset of *HiBAL* and non-BAL quasars, both with O III 5007Å EWs. Unfortunately, the wavelength limits of SDSS do not allow this. One of the problems with using just LoBAL quasars as tests of unification is that there is evidence that they are drawn from a different population than normal quasars, perhaps suggesting an *evolutionary* origin. Examples include anomalously high LoBAL fractions in dust-reddened quasar samples ([Urrutia et al. 2009](#)) and infra-red selected samples ([Dai et al. 2012](#)); although see also [Lazarova et al. \(2012\)](#)). To partially address this issue, I also build a small sample of HiBAL quasars in SDSS by cross-matching the S11 catalog with BALs identified in the HST COS archive. BALs were selected from the COS spectra using the balnicity index, BI , defined in equation ???. HST objects were designated as HiBALs by satisfying the condition that $BI > 0$ in one of CIV, NV, SiIV. The mass and Eddington fraction measurements from S11, with errorbars, are shown against the background distribution of all quasars.

Fig. 2 shows histograms of a number of different emission line properties for samples A and B. As discussed by previous authors (e.g. [Weymann et al. 1991](#)), I find that BAL and non-BAL quasars really do seem to possess very similar emission line properties. The EW is related to the ‘face-on’ equivalent width, EW_0 by the equation

$$EW = EW_0 / \epsilon(\theta) \quad (1.1)$$

where θ is the viewing angle with respect to the symmetry axis and $\epsilon(\theta)$ is the ‘angular emissivity function’, which describes how the continuum luminosity from the disc varies as a function of viewing angle. For a foreshortened disc this is simply $\epsilon(\theta) = \cos \theta$.

Thus, if BAL quasars are viewed from a larger viewing angle on average then one would expect them to possess higher EWs, with a broader distribution. It is already apparent from figure 1 that the BAL distribution mean is not systematically higher than the non-BAL mean – in fact, it is lower. This is not expected from a model in which the continuum is foreshortened and BAL outflows are at all equatorial. This problem is examined further in section 1.4. First, I will examine the motivations for different forms of $\epsilon(\theta)$ in AGN and quasars.

1.3 The Angular Distribution of Emission from an Accretion Disc

As introduced in chapter 1, the most widely-used theoretical model for an accretion disc is the so-called ‘ α -disc’ model of SS73. There are a number of well-documented problems when fitting AGN SEDs with SS73 accretion disc models (see section ??), Despite these problems, Capellupo et al. (2015) recently had some success fitting spectra of AGN when the effects of GR, mass-loss and comptonisation were included. In this section, I start by discussing the angular distribution of emission from an SS73 disc, before discussing opacity and GR effects. In order to explore these effects, I use AGNSPEC (Hubeny et al. 2000; Davis & Hubeny 2006; Davis et al. 2007). I stress that the discussion here is not limited to SS73 discs; the only real condition for the expected angular distributions derived here is that the disc is geometrically thin and optically thick.

1.3.1 Standard Thin Disc Models

Any geometrically thin, optically thick disc will appear foreshortened and limb darkened (if temperature decreases with height from the central disc plane). Foreshortening is a simple $\cos \theta$ geometric effect, where θ is the inclination with respect to the vertical z axis, which is perpendicular to the disc plane. Limb darkening, $\eta(\theta)$, is given by

$$\eta(\theta) = a(1 + b \cos \theta), \quad (1.2)$$

where a is a normalisation constant and b governs the strength of the limb darkening. $b = 3/2$, known as the Eddington approximation tends to give good agreement with solar observations (e.g. Mihalas 1978). The two effects can be combined to give an angular emissivity function, of

$$\epsilon(\theta) = a \cos \theta \left(1 + \frac{3}{2} \cos \theta\right). \quad (1.3)$$

1.3.2 Including GR, Comptonisation and Opacity Effects

In reality, limb darkening is not frequency independent and depends on the bound-free and bound-bound opacities in the disc. In addition, it has been shown that GR can

‘isotropize’ the radiation field in XRBs (Zhang et al. 1997; Muñoz-Darias et al. 2013), in some cases overcoming foreshortening effects. To assess the impact of GR and disc opacities on $\epsilon(\theta)$ I use AGNSPEC models, which uses stellar atmosphere calculations to calculate the SED in a series of annuli, before using the KERRTRANS code to calculate the emergent SED by ray-tracing along Kerr geodesics. Fig. 1.3 shows $\epsilon(\theta)$ as a function of θ for AGNSPEC models for minimally and maximally spinning BHs, compared to foreshortened and limb-darkened predictions for SS73 models. Clearly, there is very little effect; the accretion disc is still strongly anisotropic in the relevant wavebands.

1.4 Predicted EW Distributions Compared to Observations

1.4.1 Fitting the Quasar Distribution

Risaliti et al. (2011, hereafter R11) analysed the EW[O III] distribution of 6029 quasars in SDSS DR5. They demonstrated that a foreshortened disc and isotropic O III 5007Å line produces a high EW tail to the distribution with a characteristic slope of $\Gamma_{EW} = -3.5$. In order to first reproduce their result and discuss its implications, I have created a sample according to their selection criteria. The criteria are that the object in question lies in the redshift range 0.01 to 0.8, have an absolute magnitude $M_i > 22$, an apparent magnitude $m_i > 19.1$, and signal to noise per pixel of greater than 5. Using the updated SDSS quasar sample of S11, this defines a sample of 14,424 quasars.

To fit the distribution, I conduct the following procedure, which is similar to the method R11 use to demonstrate that the power law tail is expected.

1. A set of isotropic angles is chosen such that $P(\theta) \propto d\Omega(\theta)$. If $\theta < \theta_1$ then the fake object is designated as unobsured, and otherwise the object is ignored.
2. To be included in the sample, the object also has to survive a selection test to simulate the distribution of angles in a flux-limited sample. This is done by drawing a random sample from the real quasar sample, and calculating a ‘doubly observed continuum flux’, F_O at 5100Å (rest frame), such that $F_O = F_{5100} \epsilon(\theta)$. The flux

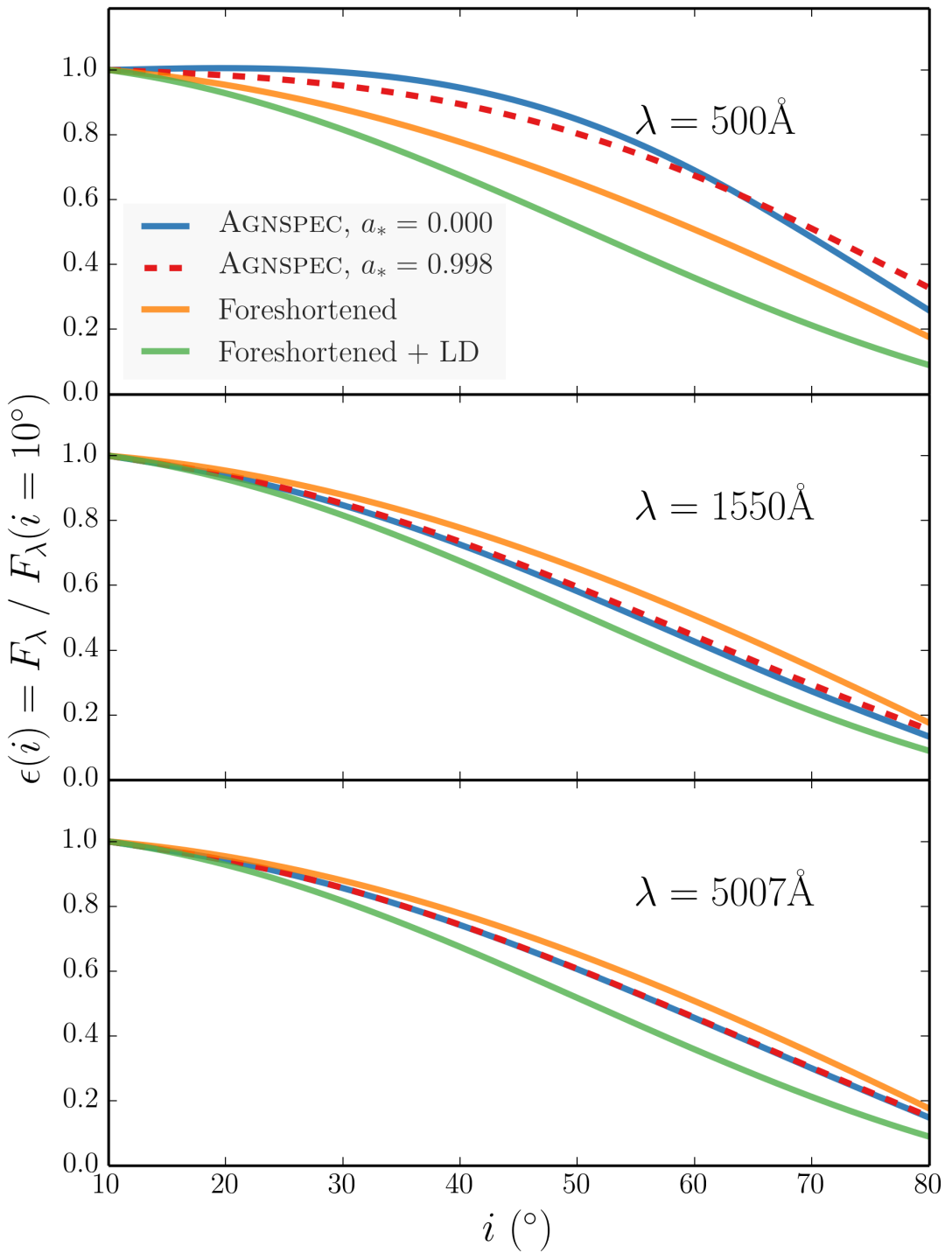


FIGURE 1.3: Monochromatic continuum luminosities from AGNSPEC and classical thin disc models.

limit is set at 5×10^{-13} erg s $^{-1}$ cm $^{-1}$ Å $^{-1}$, but the results are fairly insensitive to the limit chosen.

3. For each mock sample, an EW_* is drawn from an intrinsic (i.e. ‘face-on’) EW distribution for quasars. This is assumed to be a gaussian. The mean, μ_* , and width, σ_* , of this Gaussian can either be set arbitrarily – for example, to demonstrate trends in mock data – or obtained from a χ^2 fit to the observed EW distribution.
4. A mock EW is estimated such that $\text{EW} = \text{EW}_0/\epsilon(\theta)$, and this process is repeated to build up a mock sample of 10^6 objects.

The result of this numerical experiment is, as found by R11, a distribution with a high EW tail of slope -3.5 . We can now vary the maximum angle, θ_1 , and examine how this tail changes. Mock data for a series of cutoff angles is shown in Fig. 1.4, for two intrinsic Gaussians. The power law behaviour is only seen when the maximum angle is sufficiently large, and a rapid decay in the distribution is observed at a characteristic EW related to both the width and mean of the intrinsic distribution as well as the cosine of the maximum angle. The top panel has μ_* and σ_* of the R11 Model 1, whereas the bottom panel shows a narrower distribution to illustrate the earlier onset of the high EW cutoff. In principle, this cutoff could be used to infer information about the viewing angle distribution of quasars, but this is complicated by poor statistics in the tail, selection effects and lack of knowledge about the true face-on distribution.

Fig. 1.5 shows the result of a χ^2 minimization fit to the R11 sample. The best fit is achieved with a maximum angle of $\theta_1 = 84^\circ$ and a slightly broader intrinsic distribution than model 1 of R11. I adopt linear binning to facilitate easy comparison with R11, and only fit up $\text{EW} = 100\text{\AA}$ due to poor statistics above that limit. Unfortunately, this makes inferring any information about a potential high EW cutoff difficult as a more complete sample at high EW is required.

1.4.2 Comparing non-BAL and BAL Distributions

In order to compare the observed distributions to those expected for BALs and non-BALs I repeat the process described in section 1.4.1 with a few key differences

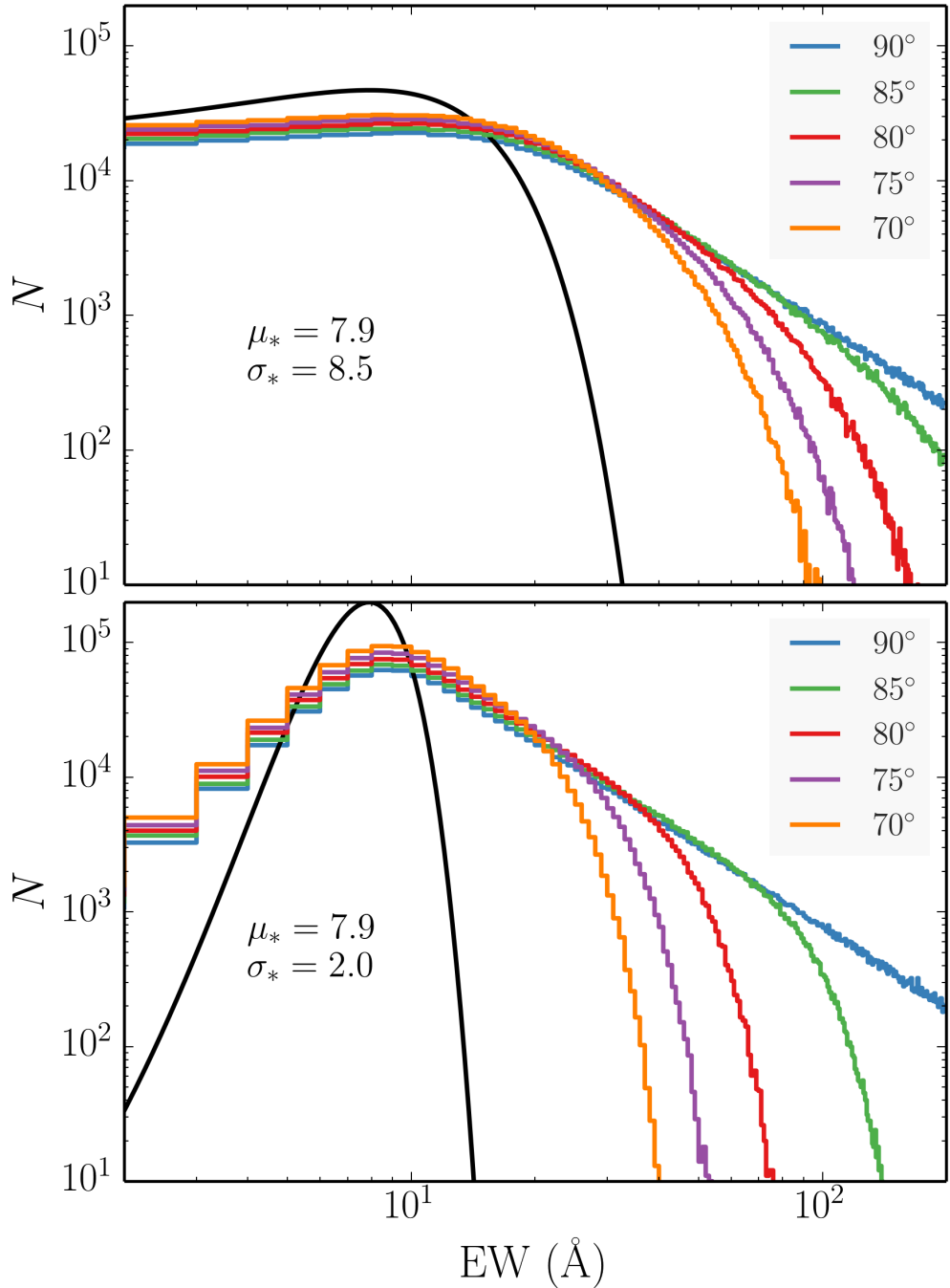


FIGURE 1.4: Theoretical Ew distributions from the numerical experiment described in section 1.4.1 for a few different maximum angles. The results in the top panel use the same intrinsic distribution as Model 1 from R11 (shown in black), whereas the bottom panel shows the distributions obtained from a narrower intrinsic Gaussian. By the time the maximum angle is limited to around 70° the cutoff is clear even at moderate values of EW.

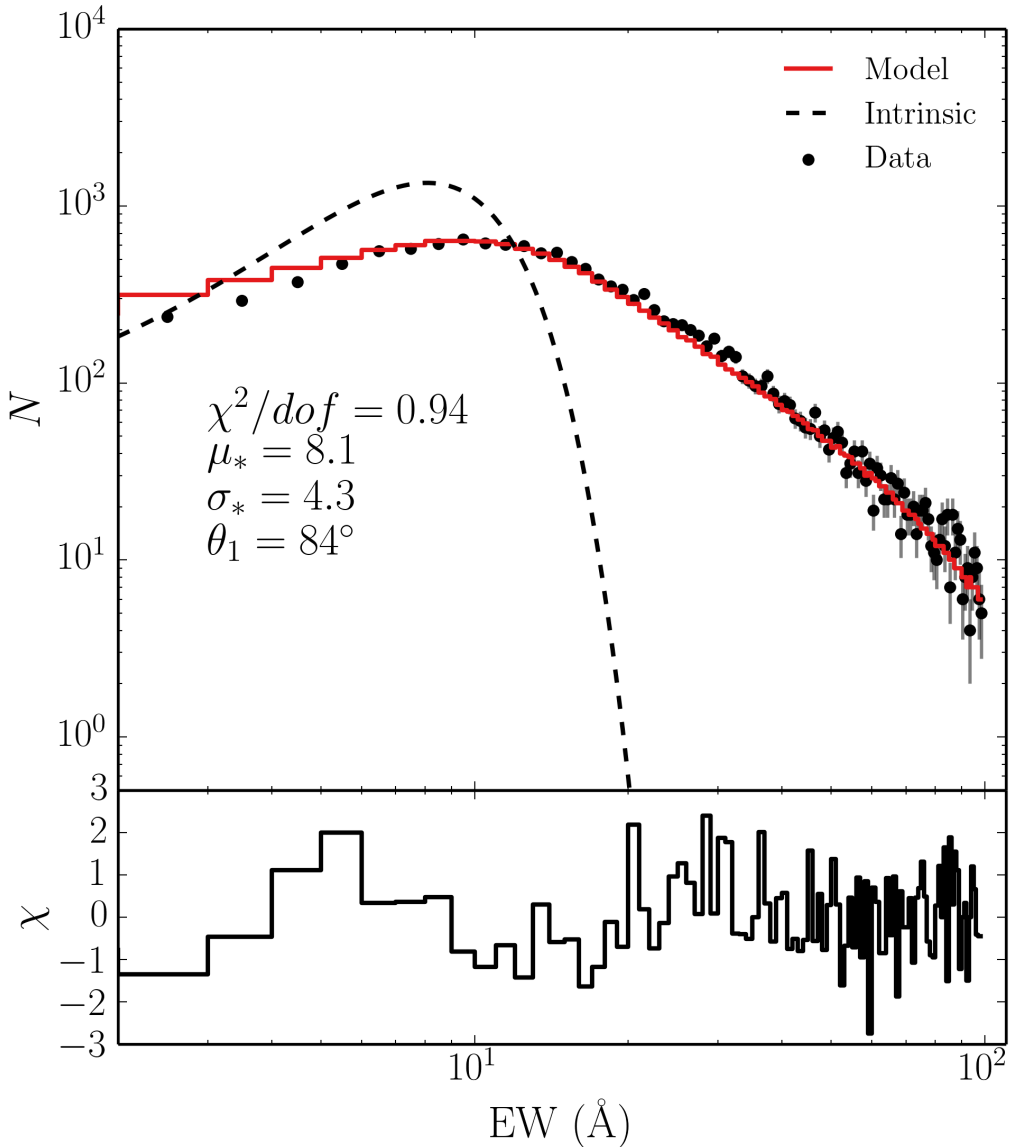


FIGURE 1.5: The EW distribution of quasars in the R11 sample (red errorbars) and the best fit model with a maximum viewing angle of 84° .

I assume $\epsilon(\theta) = \cos \theta$, as this is the conservative estimate from section 1.3. The Monte Carlo simulation undergoes the following steps:

1. A set of isotropic angles is chosen such that $P(\theta) \propto d\Omega(\theta)$. If $\theta_{min} < \theta < \theta_{max}$ then the fake object is flagged as a mock BAL. If $\theta < \theta_{min}$ then the fake object is designated a non-BAL, and otherwise the object is ignored. To be included in the sample, the object also has to survive a selection test based on a arbitrary flux selection limit, to simulate the distribution of angles in a flux-limited sample.

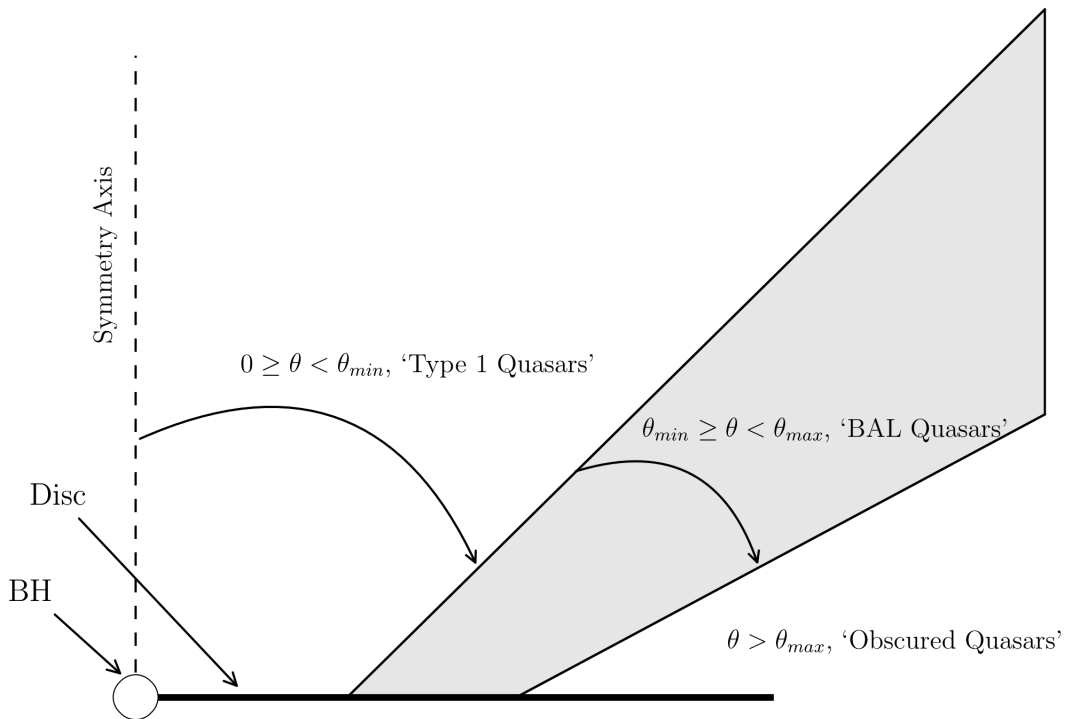


FIGURE 1.6: The geometry of the toy model used to carry out the Monte Carlo simulations

2. I then construct a best estimate of the intrinsic (i.e. ‘face-on’) EW distribution for non-BAL quasars. This is done via a χ^2 minimisation, by finding the gaussian with μ and σ which best reproduces the observed distribution when convolved with the non-BAL angles generated in the previous step. a χ^2 minimisation.
3. For each mock sample, a EW_0 is drawn from the intrinsic gaussian.
4. A mock EW is estimated such that $EW = EW_0/\epsilon(\theta)$, and this process is repeated to build up a mock sample of objects.
5. The number of objects in the mock sample with $\theta_{min} < \theta < \theta_{max}$ is recorded, providing an estimate of the expected BAL fraction for this wind geometry. This already includes a selection effect for the weaker continuum flux.
6. The value of the K-S test statistic is recorded, in which the mock BAL sample is compared to the real BAL sample. The mean and variance of the mock sample is

also recorded. This allows us to ascertain which regions of parameter space best fit the observed BAL distribution

This process is repeated for a grid of θ_{min} and θ_{max} . The results are shown in figure 1.7, in which the mean, standard deviation and f_{BAL} are shown as a function of θ_{min} and θ_{max} . First, I find that the quasar EW distribution cannot be well-fitted unless quasars are viewed from a wide range of angles, right up to edge-on. The best fit is obtained for $\theta_{min} = 85^\circ$ and is shown in Fig. 1.5.

Although the quasar EW distribution can be fitted with the above model, neither the true distribution of viewing angles or the intrinsic ‘face-on’ EW distribution of the emission line in question is known. If an intrinsic, face-on distribution could be constructed then the Kolmogorov-Smirnov test and χ^2 minimization could be used to place constraints placed on BAL and non-BAL viewing angles. Furthermore, the distribution of C IV quasar EW cannot

Despite these difficulties, it is still relatively easy to demonstrate that the EW distribution in BAL quasars is not well produced by a model in which the accretion disc is foreshortened and BAL quasars are viewed from high inclinations. I will show this by conducting a simple Monte Carlo experiment to ascertain which geometries best reproduce the observed distributions. Throughout these simulations,

1.4.3 EW[O iii] in LoBAL quasars

As expected, equatorial viewing angles are strongly disfavoured, and furthermore, it is only possible to fit the tail to the EW[O III] distribution if non-BAL quasars are allowed to be viewed from high inclinations. However, any conclusions are somewhat limited by the lack of knowledge about the intrinsic face-on distribution of EW[O III], or equivalently, the orientations of the quasars themselves. If either of these quantities were known then specific viewing angles of BAL outflows could be

An additional limitation is due to the SDSS wavelength coverage and means that only LoBALs can be used when EW[O III] is present. I would suggest that future observational programs might look to build up a large sample of EW[O III] measurements for HiBAL quasars. In the mean time, I will turn to the UV broad emission lines to examine if the above conclusions also hold sway when it is possible to consider HiBAL quasars.

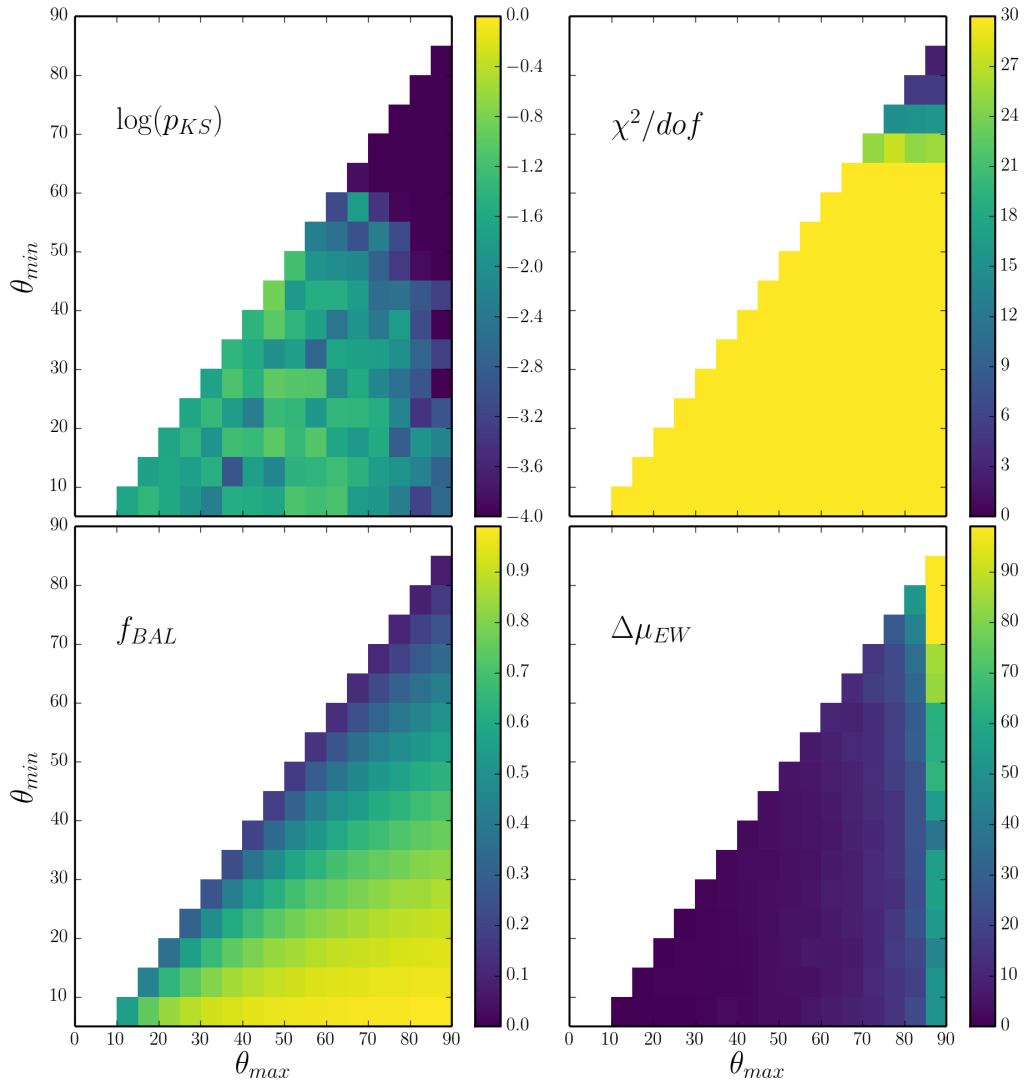


FIGURE 1.7: Heatmap showing the results

1.4.4 Broad Emission Lines in HiBAL quasars

The situation involving broad emission lines is somewhat different, as the lines are dipole permitted transitions and can thus be optically thick.

1.5 Discussion

I have demonstrated that the EW distributions of the O III 5007Å emission line in quasars is not consistent with a model in which BAL quasars are viewed from equatorial angles and the continuum emission originates from a foreshortened accretion disc. This conclusion would be strengthened were I to include limb darkening. This conclusion

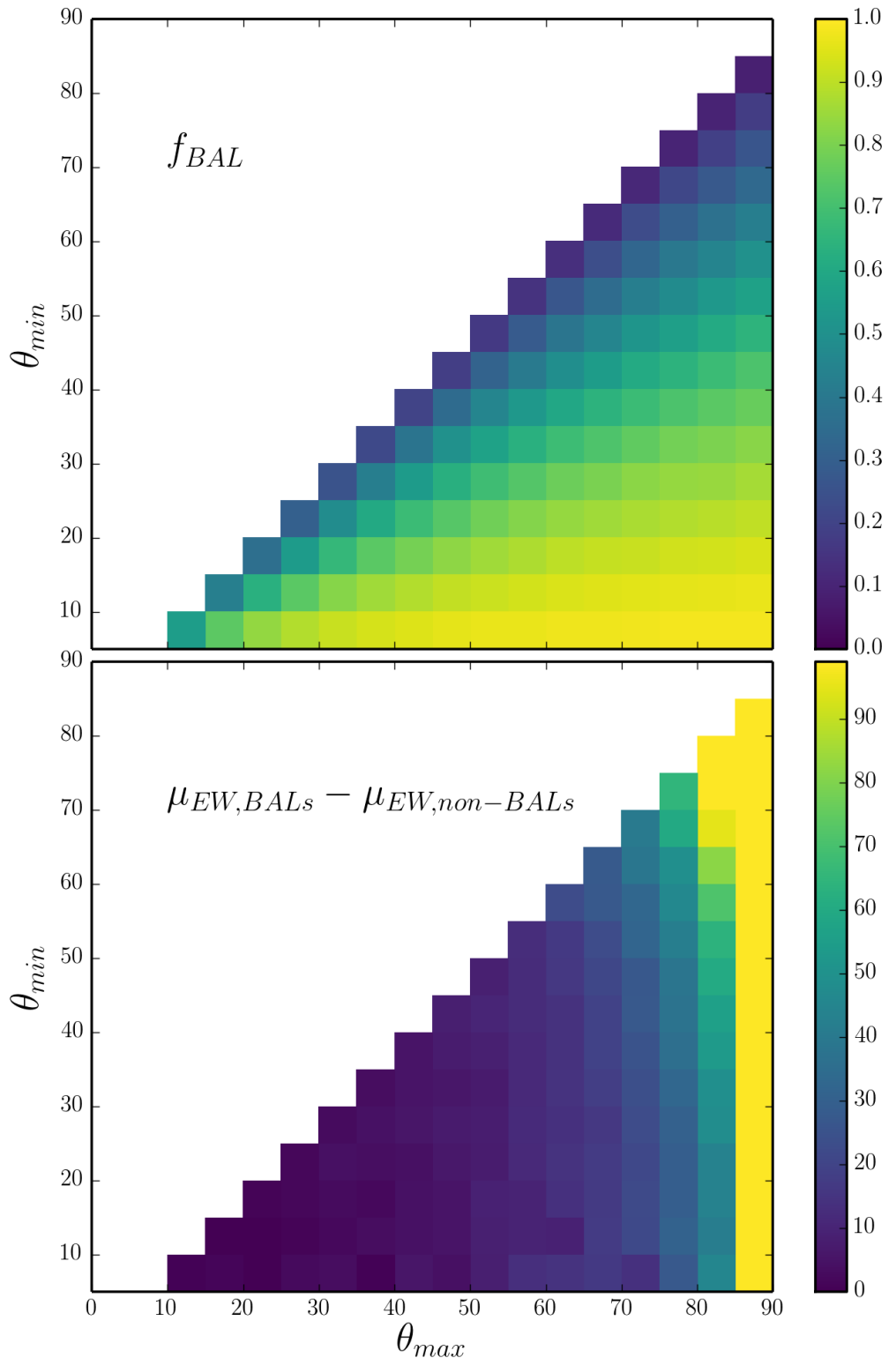


FIGURE 1.8: Contour plots from the Monte Carlo simulations.

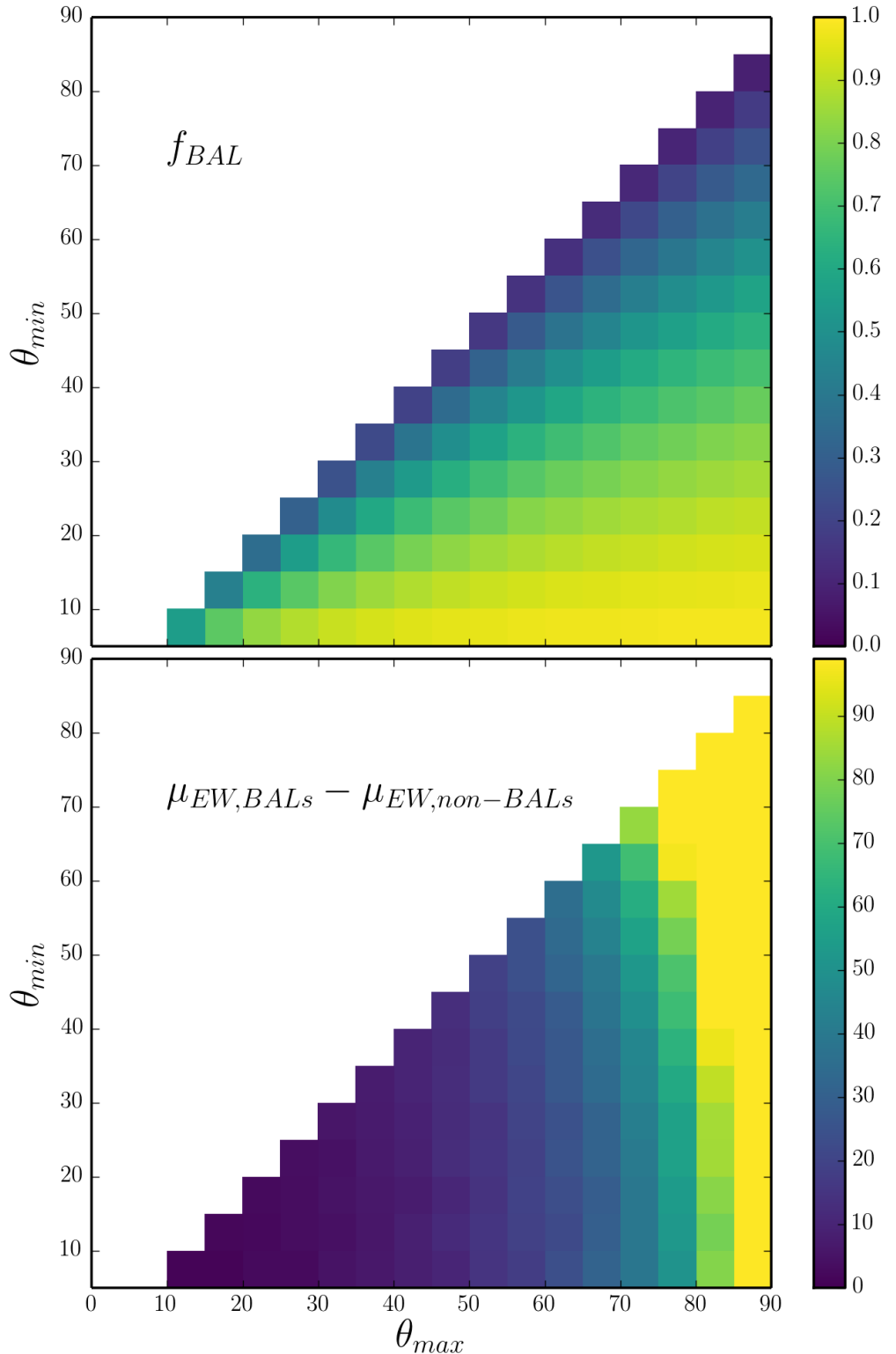


FIGURE 1.9: Contour plots from the Monte Carlo simulations.

Par. A	Par. B	$r_{corr,AB}$ (non- BALs)	$r_{corr,AB}$ (BALs)
$\log[\text{EW}[\text{O III}]]$	$\text{FWHM}[\text{H}\beta]$	0.14	0.18
$\log[\text{EW}[\text{O III}]]$	R_{FeII}	-0.51	-0.67
$\text{FWHM}[\text{H}\beta]$	R_{FeII}	-0.26	-0.42

TABLE 1.1: Eigenvector 1 correlation coefficients

is extendible to the broad emission lines, with the caveat that those lines are dipole transitions and so opacity effects can change the angular distribution of emission. I will now explore how the above results compare to other observations of quasars that are expected to probe system orientation.

1.5.1 Eigenvector 1

Eigenvector 1 (EV1) is a fundamental parameter space for AGN and quasars (Boroson & Green 1992; Sulentic et al. 2000; Marziani et al. 2001; Shen & Ho 2014). It relates the FWHM of H β , FWHM[H β], the relative iron strength, R_{FeII} and the EW[O III]. Both EW[O III] and FWHM[H β] have been used as orientation indicators, and so comparing the BAL EV1 distribution to the non-BAL EV1 distribution is particularly interesting.

Fig. 1.10 shows the quasar distribution from sample A in EV1 parameter space, with BAL quasars from samples A and B overplotted. (Shen & Ho 2014, hereafter SH14) propose that the main inclination driver in the parameter space is FWHM[H β], and that high inclination sources should thus cluster around a diagonal line from the lower right to upper left quadrants. Conversely, R11's analysis instead suggests that high inclination sources should cluster around high EW OIII widths. As EW[O III] and FWHM[H β] are very weakly correlated (Spearman's rank coefficient of 0.13), this means they should lie to the left of the parameter space. Inspection of the figure clearly shows that BAL quasars are not only found in one region of the EV1 parameter space.

In order to assess this more quantitatively, I have shown contours of quasar counts overlaid on the scatter plot. The contours correspond to the number of objects in each bin, where the bins are of size $\Delta R_{\text{FeII}} = 0.2$ and $\Delta \text{FWHM}[\text{H}\beta] = 500 \text{km s}^{-1}$. The percentage of quasars falling within the inner contour is 45%, whereas only 18% of BAL quasars fall in the space. Conversely, 24% of BAL quasars fall outside the outermost contour compared to 10% of non-BAL quasars. It would therefore appear that BAL quasars are

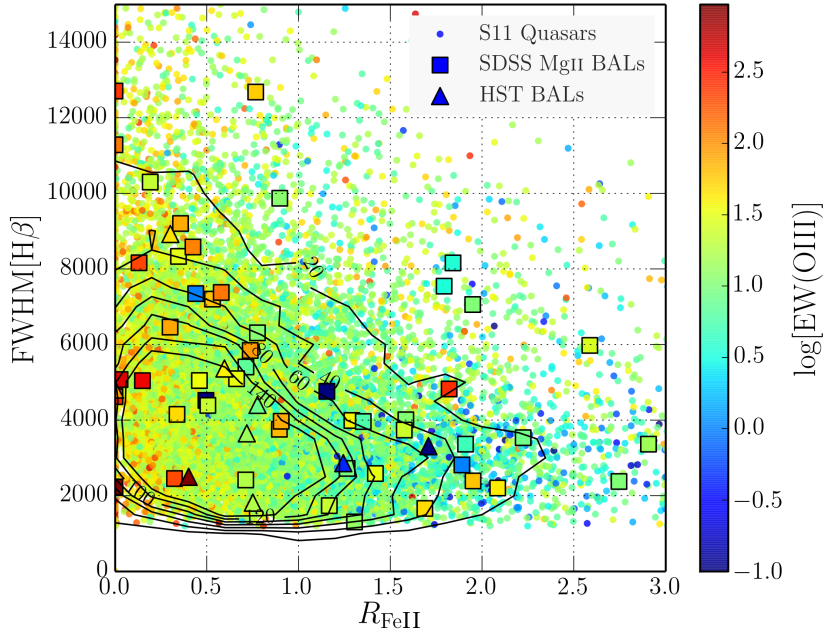


FIGURE 1.10: Eigenvector 1 for BAL and non-BAL quasars. FWHM of the $\text{H}\beta$ line plotted against the relative iron strength, R_{FeII} . The colour coding corresponds to the EW of OIII. The dots mark all quasars from sample A, while the squares mark those with Mg II BALs. The triangles show the HST BAL quasars from sample B.

preferentially clustered towards the high-mass and high-inclination end of EV1 space (under the interpretation of SH14). This is further illustrated by Fig. 1.11, which shows the LoBAL fraction in the same bins, compared to the mean LoBAL fraction. This is again suggestive of an overdensity towards the upper right of the parameter space. It is also clear that a unification picture in which BAL quasars are viewed exclusively from high inclinations is ruled out, under both the R11 and SH14 interpretations.

Larger datasets, preferably including HiBAL quasars with EV1 measurements, are needed in order to properly constrain the EV1 behaviour of BAL quasars. However, overall, the behaviour of $\text{FWHM}[\text{H}\beta]$ strengthens the above conclusion that BAL quasars are not always viewed from extreme inclinations.

1.5.2 Radio Observations

Fig. ? shows the equivalent width distributions in radio-loud quasars, split into core or lobe dominated. This designation is commonly used as an orientation indicator (Orr & Browne 1982; Wills & Brotherton 1995). Although th

In this case, we can see that A full investigation of this is beyond the scope

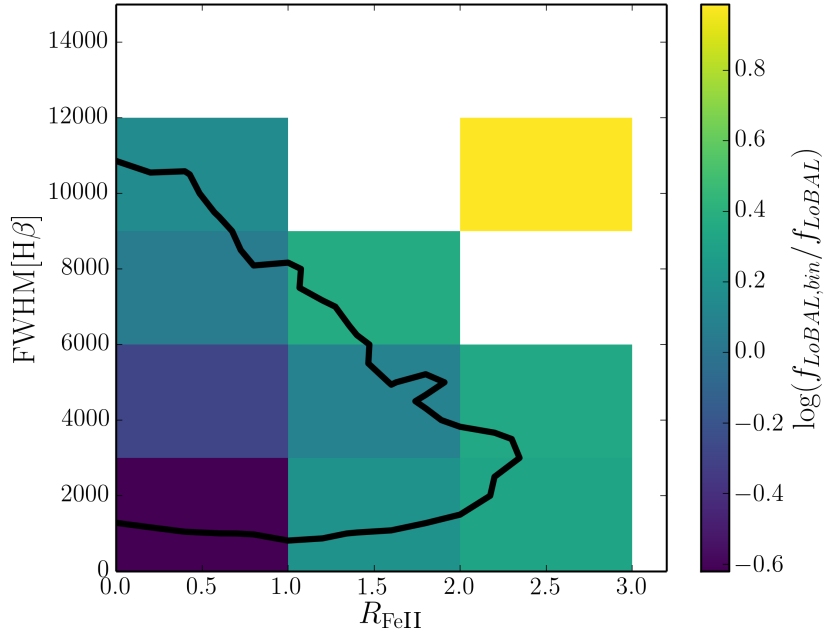


FIGURE 1.11: LoBAL fraction compared to mean LoBAL fraction in Eigenvector 1 space. The contour shows the outermost contour from Fig. 1.10 for reference.

1.5.3 Polarisation

Polarisation measurements of BAL quasars tend to show two properties. The first is a polarisation angle of $\gtrsim 60^\circ$ with respect to the radio jet axis in RL source (Brotherton et al. 2006). The second is a polarisation percentage of around 2.4 times greater, on average, than the non-BAL population. The polarisation percentages of a sample of BAL quasars from REF are compared to the Type I and Type II AGN populations from REF in Fig. 1.12.

The polarisation properties of BAL quasars offer some of the best insights into the geometries of BAL outflows, some of which appear to be in contrast with the conclusions drawn from emission line and radio properties.

1.5.4 Theoretical Considerations

Discuss Proga models: They tend to rise fairly equatorially (see eg. PK04) Talk to Nick?

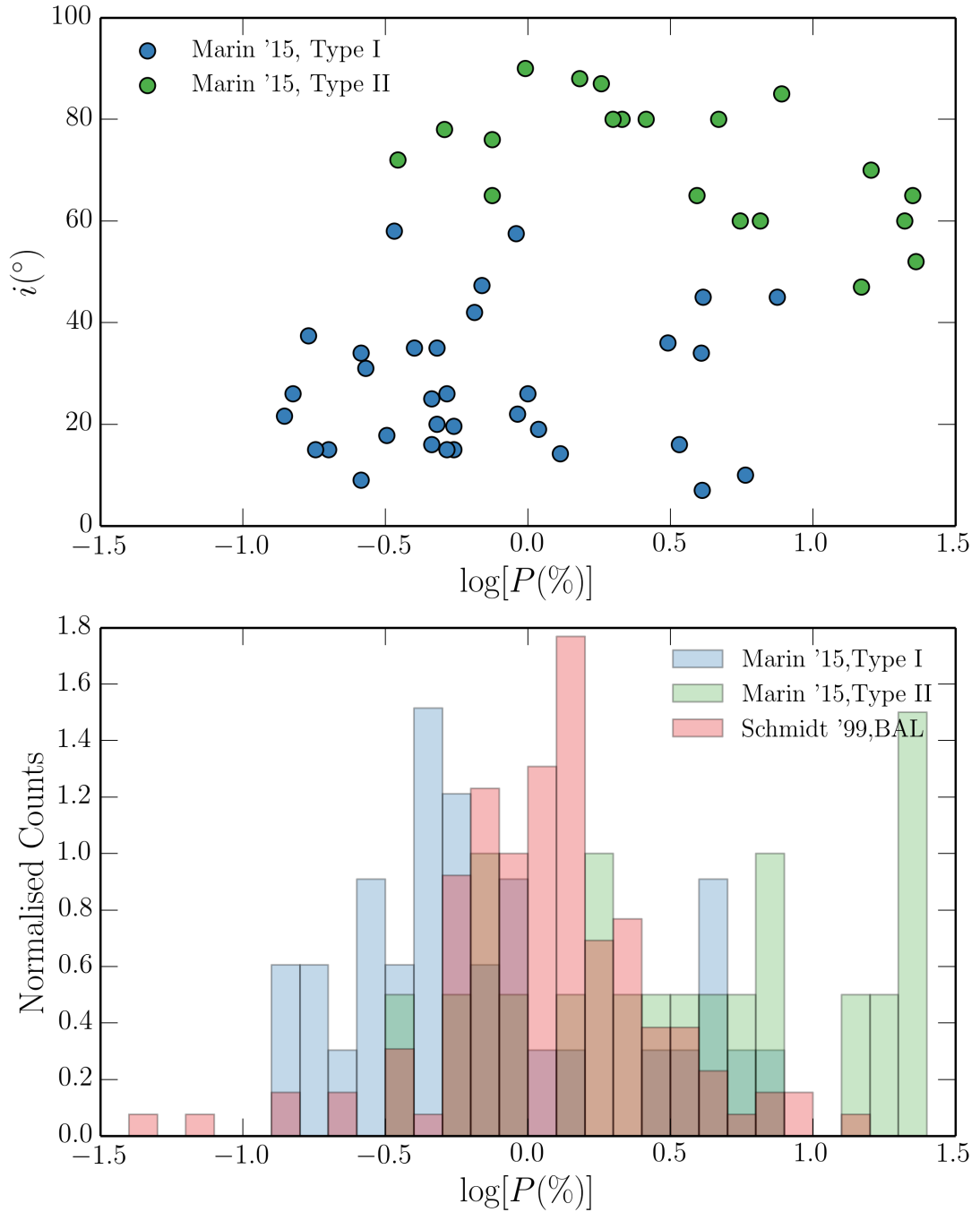


FIGURE 1.12: *Top:* Polarisation percentages as a function of measured inclination from Marin et al. (2015) for Type I and Type II AGN. *Bottom:* Histograms of polarisation percentages for BAL quasars from Schmidt et al. (1999) together with the Marin et al. (2015) AGN sample.

1.6 Conclusions

I have explored the emission line properties of BAL and non-BAL quasars and found that they are inconsistent with a unification picture in which BAL outflows rise equatorially from a foreshortened or limb darkened accretion disc. Based on these findings, it is possible to construct a few possible scenarios that are not ruled out by the above results. These conclusions have the caveat that I have assumed that conclusions drawn about LoBAL quasars can be extended to BAL quasars in general.

- *Scenario 1:* The quasar continuum is roughly isotropic, which is not expected from a geometrically thin, optically thick accretion disc. I have demonstrated that general relativistic effects cannot account for this discrepancy in the UV. Reprocessing by surrounding dense plasma with a large covering factor or limb brightening in the disc may provide possible explanations which this analysis cannot yet confirm or refute.
- *Scenario 2:* Quasar discs are strongly anisotropic, as expected from a geometrically thin, optically thick accretion disc. In this case, BAL outflows cannot only emerge at extreme inclinations and should instead be seen at very similar angles to non-BAL quasars. Polarisation measurements need to be reconciled with this hypothesis. I recommend that future RT modelling efforts explore different outflow geometries and that detailed polarisation modelling is undertaken to constrain the outflow opening angles.
- *Scenario 3:* The geometric unification model does not explain the incidence of BALs in quasars, or requires an additional component which is *time-dependent*, such as an evolutionary or accretion state origin for BAL outflows. In this scenario, BAL quasars would be seen from very similar angles to non-BAL quasars. However, the evidence for this is limited and there is no good model for why outflows would exist only for $\sim 20\%$ of a quasar's lifetime. Even if this is the case, then the covering factor of the outflow still needs to be constrained in order to estimate the BAL duty cycle.

Regardless of the conclusions about BAL quasars and their outflow geometries, this analysis allows conclusions to be drawn about the *overall* quasar population. In scenario

1, the EW[O III] distribution of quasars cannot be driven by inclination as suggested by (Risaliti et al. 2011). It is also clear from the work presented here that $\log R$, EW[O III] and FWHM H β are *cannot all* be reliable orientation indicators. Furthermore, if a geometric unification does explain BAL quasars, then absorption effects cannot be responsible for the observed EW[O III] distribution. The above conclusions each pose a different challenge to the current understanding of, respectively, accretion physics, polarisation measurements and geometric unification models. This work therefore adds to the growing evidence that our simplest models are not sufficient to describe the overall quasars and that alternatives should be sought.

Chapter 2

Conclusions and Future Work

“...and the credits rave as the critics roll.”

Mike Vennart, *Silent/Transparent*

I began this thesis with the fundamental tenet that accreting systems and their associated outflows are astrophysically important. However, I also demonstrated that much of the diverse phenomenology associated with such systems, as well as the underlying *physics*, is not well understood. Having attempted to address some of the issues raised in the introductory chapters, I will provide some concluding remarks. First, I will summarise my findings, before commenting on how future research can help unveil the true nature of accretion discs and their winds.

A large portion of this PhD has been spent maintaining, testing and developing the MCRT and ionization code, PYTHON. The first step in this project was to understand the macro-atom scheme developed by Lucy (2002, 2003), and its specific integration into PYTHON. I described the scheme and the operation of PYTHON in detail in chapter 3, partly in the hope that it will prove a useful document for future efforts involving this useful, but complex, piece of software. The latter parts of the same chapter focused on the series of tests I conducted to robustly verify that the code worked as expected and that it could reproduce the analytical and computational results in the right physical limits. Near the start of the project many of these tests would fail, either because PYTHON did not possess the relevant atomic data, or because the necessary integration between the macro-atom and simple-atom portions of the code was not yet in place.

Thus, while time consuming, progressing to the point where all the tests shown in chapter 3 could be passed was an important milestone, and enabled the techniques in question to be applied to astrophysical problems with confidence.

The first of these astrophysical problems involved CVs, and in particular those accreting at a relatively high rate, such as DNe or NLs. Having improved the radiative transfer techniques from previous CV modelling efforts involving PYTHON (LK02, ?), it was now possible to see if the outflows that are responsible for the P-Cygni profiles seen in UV resonance lines could also affect the *optical* line and continuum emission. The results are unambiguous. By simply taking the SV93/LK02 models – designed to reproduce the UV spectra of high-state CVs – and ‘turning on’ the improved radiative transfer mode, the wind has a significant effect on the optical spectrum, producing strong H α , He II $\lambda 4686\text{\AA}$ and He II 3202\AA lines, among others, at high inclinations.

I then conducted a small parameter search over just two kinematic parameters, to see if a model could produce *all* of the optical H and He lines observed in high-state CVs. Synthetic spectra from a model with a more slowly accelerating outflow show the full sequence of H and He recombination lines, with the observed trend from strong emission at high inclination to weaker lines at low inclination. Furthermore, the dense outflow now produces strong Balmer recombination emission that is sufficient to ‘fill in’ the Balmer absorption edge intrinsic to the disc atmosphere input spectrum. The optimised model is not without issues; the red wing to the C IV line is now overly strong, particularly at high inclinations, and He II emission is stronger than that observed. Nevertheless, the synthetic spectra exhibit reasonable verisimilitude with observations of the high inclination NL RW Tri, and the results indicate that disc winds may have a much broader impact, especially in wavelength terms, than is traditionally expected. Furthermore, the large vertical extent of the line emitting region has implications for techniques that assume planar line emission, such as Doppler tomography (e.g. [Marsh & Horne 1988](#)) and eclipse mapping (e.g. [Horne et al. 1994](#)).

In chapter 5, I applied similar techniques to the question of quasar unification, but with one additional adaptation. In order to simultaneously increase the emission measure of the wind, as well as moderate the ionization state in the presence of strong X-rays, I incorporated a simple treatment of clumping into PYTHON. The technique – known as *microclumping* – is prevalent in the stellar wind community, but this was the first

time it had been applied to quasar winds in this context. Although the motivation for including clumping was in some sense empirical, in that H13 could not produce a model with strong C IV BALs without severely limiting the X-ray luminosity, the validity of this approach is strengthened by the theoretical and observational evidence for clumping in line-driven hot star winds (see section ?? and ??).

Once again, I conducted a parameter search, this time in 5 dimensions. A broad family of models produce strong UV emission lines at low inclinations and UV BALs at high inclinations. Thus, the first success of the clumpy quasar wind model is that, for clumping factors comparable to those required in stellar wind modelling (Hamann et al. 2008), the ionization state of the wind matches well with observations despite the presence of strong X-ray radiation. Indeed, the X-ray properties of the model now agree well with observed non-BAL and BAL quasar values for L_X , suggesting that the partially self-shielding BAL outflow itself might be responsible for the observed X-ray weakness of BAL quasars. Perhaps the most compelling attribute of the wind model is that it naturally reproduces the broad range of ionization states observed in AGN such that the wind emission has very similar characteristics to the observed BLR spectrum (see, e.g., Fig. ??). The primary limitation of the fiducial quasar model is a geometric one; it is not possible to produce comparable line EWs at low inclination to those at high inclination, due to the foreshortened, limb-darkened, and absorbed disc emission. Thus, even if the low inclination line emission could be matched to the observed quasar EWs, the model would then over-predict the line emission emerging at high inclination ‘BALQSO-like’ angles. This suggests an issue with an equatorial unification model, and provides the motivation for exploring the observational characteristics of emission lines in BAL and non-BAL quasars.

The final project in this PhD saw a switch in philosophy, as, informed by the radiative transfer modelling, I turned to observations and in particular the invaluable dataset that is the *Sloan Digital Sky Survey*. The aim of this exercise was to more quantitatively assess the apparent similarity in emission line properties in BAL and non-BAL quasars. I first reproduced the results of Risaliti et al. (2011) using the updated dataset by fitting the distribution of the EW of the O III 5007Å emission line with a simple geometric model, in which an intrinsic Gaussian distribution was convolved with the expected angular distribution of quasars expected in a flux-limited sample. I then constructed a simple toy geometric unification model, and showed that predictions from the simplest

quasar wind models – those where an equatorial outflow rises from a geometrically thin, optically thick accretion disc – are not consistent with the observed EW distributions of quasar emission lines. The results also suggest that obscuration is not the key driver of the EW[O III] distribution – albeit under the assumption that BAL quasars are drawn from the same population as non-BAL quasars.

The overall conclusions of this final study are striking, and extend far beyond just constraining BAL outflow parameters. They suggest a few possible scenarios, all of which present some problems that the data cannot yet confirm or refute.

2.1 Suggestions for Future Work

2.1.1 CVs as Accretion and Outflow Laboratories

CVs are the closest and best understood laboratories for our understanding of accretion physics. In particular, the NL variables make excellent testbeds for the α -disc model, as they are one of the few accreting systems known to lie in a relatively constant accretion rate state – fulfilling an explicit assumption of the SS73 prescription. I suggest that two observational programs relating to NLs are pursued. The first is to take broadband, simultaneous spectroscopy of a number of NL variables. This will allow the impact of winds on the spectrum to be assessed more carefully as modelling of the entire wavelength range can be undertaken, possibly including fits to the observed spectrum. It will also allow the broadband SED to be fitted with confidence, and inferences made about the temperature profile of the disc. The second is to take measurements of the depth of the Balmer jump in a relatively large sample of NLs, either through narrow band spectroscopy or two-band photometry. Together with inclination measurements the predictions of disc and outflow models can be tested directly by exploring how the depth of the Balmer absorption edge varies with viewing angle and accretion rate.

2.1.2 Improving the Treatment of Clumping

A few

2.1.3 Improving Atomic Models

In chapter 4, the dominant source of heating in the benchmark CV model is line heating. This means that accurate collision strengths are needed in order

2.1.4 Using Radiative Transfer to Test

2.1.5 Obtaining Reliable Orientation Indicators

A wide variety of quantities have been used as AGN orientation indicators. However, many of these indicators are *model-dependent*, which is concerning given the lack of knowledge about the true origins of the multi-wavelength AGN SED. Furthermore, I showed in chapter 6 that it is not possible for EW[O III], FWHM[H β] and radio-core dominance to *all* be reliable orientation indicators due to the lack of the expected correlations between these measurements.

In order to distinguish between geometric unification, obscuration and evolutionary scenarios for the diversity of AGN it is critical to constrain their inclinations.

2.1.6 Placing BAL Quasars on the Eigenvector 1 Parameter Space

2.2 Closing Remarks

Above all, this work demonstrates that *disc winds matter*. They are ubiquitous in accreting systems and appear to have a profound connection with the accretion process.

Bibliography

- Borguet B. C. J., Edmonds D., Arav N., Dunn J., Kriss G. A., 2012, ApJ 751, 107
- Boroson T. A., Green R. F., 1992, ApJs 80, 109
- Brotherton M. S., De Breuck C., Schaefer J. J., 2006, MNRAS 372, L58
- Capellupo D. M., Netzer H., Lira P., Trakhtenbrot B., Mejía-Restrepo J., 2015, MNRAS 446, 3427
- Dai X., Shankar F., Sivakoff G. R., 2012, ApJ 757, 180
- Davis S. W., Hubeny I., 2006, ApJs 164, 530
- Davis S. W., Woo J.-H., Blaes O. M., 2007, ApJ 668, 682
- DiPompeo M. A., Brotherton M. S., Cales S. L., Runnoe J. C., 2012a, MNRAS 427, 1135
- DiPompeo M. A., Brotherton M. S., De Breuck C., 2012b, ApJ 752, 6
- Hamann W.-R., Oskinova L. M., Feldmeier A., 2008, in W.-R. Hamann, A. Feldmeier, L. M. Oskinova (eds.), Clumping in Hot-Star Winds, 75
- Horne K., Marsh T. R., Cheng F. H., Hubeny I., Lanz T., 1994, ApJ 426, 294
- Hubeny I., Agol E., Blaes O., Krolik J. H., 2000, ApJ 533, 710
- Lazarova M. S., Canalizo G., Lacy M., Sajina A., 2012, ApJ 755, 29
- Lucy L. B., 2002, A&A 384, 725
- Lucy L. B., 2003, A&A 403, 261
- Marsh T. R., Horne K., 1988, MNRAS 235, 269

- Marziani P., Sulentic J. W., Zwitter T., Dultzin-Hacyan D., Calvani M., 2001, ApJ 558, 553
- Mihalas D., 1978, Stellar atmospheres /2nd edition/
- Muñoz-Darias T., Coriat M., Plant D. S., Ponti G. et al., 2013, MNRAS 432, 1330
- Orr M. J. L., Browne I. W. A., 1982, MNRAS 200, 1067
- Proga D., 2005, in J.-M. Hameury, J.-P. Lasota (eds.), The Astrophysics of Cataclysmic Variables and Related Objects, Vol. 330 of *Astronomical Society of the Pacific Conference Series*, 103
- Risaliti G., Salvati M., Marconi A., 2011, MNRAS 411, 2223
- Shen Y., Ho L. C., 2014, Nature 513, 210
- Shen Y., Richards G. T., Strauss M. A., Hall P. B. et al., 2011, ApJs 194, 45
- Sulentic J. W., Zwitter T., Marziani P., Dultzin-Hacyan D., 2000, ApJ Letters 536, L5
- Urrutia T., Becker R. H., White R. L., Glikman E. et al., 2009, ApJ 698, 1095
- Weymann R. J., Morris S. L., Foltz C. B., Hewett P. C., 1991, ApJ 373, 23
- Wills B. J., Brotherton M. S., 1995, ApJ Letters 448, L81
- Zhang S. N., Cui W., Chen W., 1997, ApJ Letters 482, L155
- Zhou H., Wang T., Wang H., Wang J. et al., 2006, ApJ 639, 716